Construction and Building Materials 349 (2022) 128733

Contents lists available at ScienceDirect

Construction and Building Materials

journal homepage: www.elsevier.com/locate/conbuildmat

Effect of early curing and substrate preparation conditions on the physical and mechanical properties of TRM-masonry composites

Ali Dalalbashi [a,*,1], Bahman Ghiassi [b,2], Daniel V. Oliveira [c,3]

[a] ISISE, Department of Civil Engineering, University of Minho, Guimarães, Portugal
[b] School of Engineering, University of Birmingham, Birmingham, United Kingdom
[c] ISISE, Department of Civil Engineering, University of Minho, Guimarães, Portugal

ARTICLE INFO

Keywords:
Textile reinforced mortar
Curing conditions
Substrate preparation
Mechanical testing

ABSTRACT

Textile reinforced mortars (TRMs) are innovative sustainable composite materials that recently received extensive attention for strengthening of masonry structures. Understanding the mechanical performance of these composites has therefore been the subject of many recent studies. However, most of these investigations have focused on the mechanical properties of these composites under controlled laboratory conditions, and their performance under field conditions is still unknown. The critical role of substrate preparation and curing conditions on the performance of these repair systems have never been addressed before. To address this gap, this paper presents an experimental investigation on the role of these factors on the performance of two different TRM systems (a steel-based TRM and a glass-based TRM) commonly used for strengthening masonry structures. The results show the importance of these factors and the need for the identification of standard procedures for the application of these systems aiming the optimization of their performance in the field.

1. Introduction

Textile-reinforced mortar (TRM) composites have received significant attention for strengthening of masonry structures. TRMs consist of textile mesh/grids embedded in an inorganic matrix. Fibers are diverse and comprise steel, alkali-resistant glass, carbon, or basalt, to name a few [1], but leading to systems sharing the same technology. As for the matrix, lime and cementitious mortars are the most commonly used ones. Lime-based mortars are usually preferred for masonry structures due to their compatibility, sustainability, and breathability [2,3].

The effectiveness of TRMs is strongly dependent on the mortar and fiber properties, the bond at the fiber-to-mortar interface, and the bond at the TRM-to-substrate interface [4,11]. Several studies can be found in the literature on the characterization of the fiber-to-mortar bond behavior [12–14], the TRM-to-substrate bond behavior [15–21], or the mechanical response of TRMs [22–24]. However, most of these studies are performed with no specific attention to the role of curing or substrate preparation on the evolution of mechanical properties in these systems. Indeed, as presented in Table 1, in a few studies that report the actual curing and preparation conditions, different procedures were followed. Not only are these different from those that occur in the field, but their variation from lab to lab makes comparisons between different experimental data impossible.

Aiming at understanding the importance of these factors, this paper presents an experimental investigation on the effect of curing conditions and substrate preconditioning on the performance of TRM composites used for strengthening masonry structures. For this purpose, three different curing conditions and three distinct levels of substrate saturation degrees (before application of TRMs) are considered. The effect of these on the mechanical properties across scales, i.e., the constituent materials, the textile-to-mortar bond behavior, and TRM-to-masonry substrate are experimentally investigated and discussed.

2. Experimental program

2.1. Overall tests description

The experimental campaign comprised a series of material

* Corresponding author.
E-mail addresses: alidalalbashi@gmail.com (A. Dalalbashi), b.ghiassi@bham.ac.uk (B. Ghiassi), danvco@civil.uminho.pt (D.V. Oliveira).
1 https://orcid.org/0000-0003-0486-1433.
2 http://orcid.org/0000-0003-4212-8961.
3 http://orcid.org/0000-0002-8547-3805.

https://doi.org/10.1016/j.conbuildmat.2022.128733
Received 29 December 2021; Received in revised form 26 May 2022; Accepted 6 August 2022
Available online 16 August 2022

Table 1
Some of the existing single-lap shear test data on lime-based TRM composites.

Reference	Mortar	Substrate	Curing condition	Substrate condition
[5]	Pozzolanic lime	Clay brick	Laboratory condition	24 h saturation
[6]	mineral NHL	Historic brick	Laboratory Condition	–
[7]	Pozzolanic lime A pozzolanic lime B	Clay brick	Laboratory Condition	24 h saturation
[8]	Pozzolanic lime	Tuff	Laboratory condition	–
[9]	Lime pozzolanic lime	Clay Brick	Keeping wet for 28 days and 7 days in the lab	Wetting surface
[10]	Mineral NHL	Modern strong brick modern weak brick Historical brick Tuff	Kept wet (RH > 95 %) for the first 3 days	–
[11]	NHL and siliceous sand	Clay brick	Cured in temperature room	Semi-saturated
[18]	Lime	Clay brick	–	Wetting the surface

characterization tests, pull-out tests, and single-lap shear tests on the steel- and glass-based TRM specimens cured following different procedures. This section presents a detailed description of the materials, specimens preparation, curing conditions, and test methods.

The specimens are named X_Y_Z_Z', in which X relates to the test type (P: pull-out test, S: single-lap shear test). Y is connected to the curing condition of the mortar, and Z is linked to the brick moisture condition, which is used just for the single-lap shear test specimens. Y and Z are defined in Section 2.3. Z', used only for the pull-out test specimens, is related to the fiber type (St: steel cord, Gl: glass yarn). Table 2 presents the nomenclature of the specimens.

2.2. Materials

The selected materials were two commercial lime-based mortars, denoted M1 and M2, two commercial fabrics, and solid clay bricks with nominal dimensions of 200 × 100 × 50 mm^3. Mortar M1 consisted of natural hydraulic lime (NHL) and eco-pozzolan, while mortar M2 was a pure natural NHL 3.5 lime and mineral geobinder base. For details on the procedure followed for preparation of the paste, the reader is referred to [4].

The steel cord used as the reinforcing material was a unidirectional ultra-high tensile steel sheet with a density of 670 g/m^2 and an effective area of one cord equal to 0.538 mm^2, according to the technical datasheets. The glass fabric was a woven biaxial fabric mesh made of alkali-resistant fiberglass. According to the technical datasheets, the mesh size and area per unit length were 25 mm × 25 mm and 35.27 mm2/ m, respectively. Based on a previous study conducted by the authors [4], the average tensile strength, Young's modulus, and rupture strain of the steel cord are 2972 MPa (coefficient of variation: CoV = 8 %), 189.34 GPa (CoV = 8 %), and 1.88 % (CoV = 9 %), respectively. These values for the glass fabric were 875 MPa (CoV = 13 %), 65.94 GPa (CoV = 5 %), and 1.77 % (CoV = 10 %), respectively.

Table 2
Nomenclature of test specimens.

Objective	Test type	Mortar curing condition	Brick moisture condition	Fiber	Specimen name
Effect of curing conditions on the fiber-to-mortar bond	Pull-out	PL-1	–	Steel cord	P_PL-1_St
				Glass yarn	P_PL-1_Gl
		PL-7			P_PL-7_St
					P_PL-7_Gl
		RH-7			P_RH-7_St
					P_RH-7_Gl
Effect of different curing conditions and brick moisture content on the TRM-to-masonry bond	Single-lap shear	PL-1	D	Steel mesh	S_PL-1_D
		PL-7			S_PL-7_D
		RH-7			S_RH-7_D
		PL-1	SS		S_PL-1_SS
		PL-7			S_PL-7_SS
		RH-7			S_RH-7_SS
		PL-1	SA		S_PL-1_SA
		PL-7			S_PL-7_SA
		RH-7			S_RH-7_SA

PL-1: curing under plastic for one day; PL-7: curing under plastic and covered with damp cloths for 7 days; RH-7: curing inside a chamber room with 90 % RH; D: dry; SS: semi-saturated; SA: saturated.

2.3. Curing and conditioning methods

Three different curing conditions were considered for the mortars: (1) curing of the specimens in the laboratory (20 °C, 60 % RH) under a plastic sheet for a day (named as PL-1); (2) curing of the specimens in the laboratory (20 °C, 60 % RH) covered with damp cloths and stored under a plastic sheet for seven days (PL-7); (3) curing of the specimens inside a chamber room (20 °C, 90 % RH) for seven days (RH-7). After that, all the specimens were stored in the laboratory until the testing day. For the preparation of the single-lap shear specimens, the bricks were conditioned to three different initial moisture contents (named as D, SS, and SA, respectively) before application of the TRM system: (1) dried (in the oven for two days at the temperature of 90 °C); (b) semi-saturated; (c) saturated (immersed in water for two days). The optimum moisture content for achieving the highest flexural bond strength between clay bricks and lime mortars is expected to be in the range of 40 % and 80 % [25,26]. So, the bricks of the single-lap shear specimens with the condition of semi-saturated are immersed in water at the flatwise surface for 165 min, resulting in moisture content of nearly 60 % of saturation (see discussions in Section 3.1.2). Combined with the curing methods, dry, semi-saturated, and saturated conditions lead to nine different types of samples for the single-lap shear tests. Fig. 1 shows the overall overview of the curing conditions considered for each test.

2.4. Material characterization tests

Differential thermal analyses (DTA) were conducted with a Q600 TA Instrument apparatus to measure the hydration level of the mortar. Considering that mortar M2 was used for both the pull-out and the single-lap shear tests (as mentioned in Sections 2.5 and 2.6), DTA tests were conducted only on this mortar. For this purpose, an aluminum pan was used, and the samples were heated from 50 °C to 1000 °C at a rate of 10 °C/min with 100 ml/min of N_2 flow [27–29]. All DTA samples (25 mg) were extracted from the center of cubic (50 × 50 × 50 mm^3) specimens. The age of DTA samples were 1, 7, and 60 days.

The compressive and the flexural strength of the mortars M1 and M2 were determined based on ASTM C109 [30] and EN 1015-11[31]. The compressive specimens were cubic (50 × 50 × 50 mm^3), and the flexural specimens had prismatic shape (40 × 40 × 160 mm^3). In addition, the tensile splitting strength and the elastic modulus of the mortars were characterized according to EN 12390-13 [32] and ASTM C496 [33] using cylindrical specimens with a 70 mm diameter and 150 mm height. All the specimens were tested at the age of 60 days, five specimens were tested at each curing condition, leading to a total of 120 specimens (2 × 4 × 3 × 5).

The mechanical properties (compressive and flexural strengths and elastic modulus) of the bricks were measured according to ASTM C67 [34], EN 1015-11 [31], and EN 12390-13 [32], respectively. For the compression tests, cubic brick samples with dimensions of 40 × 40 × 40

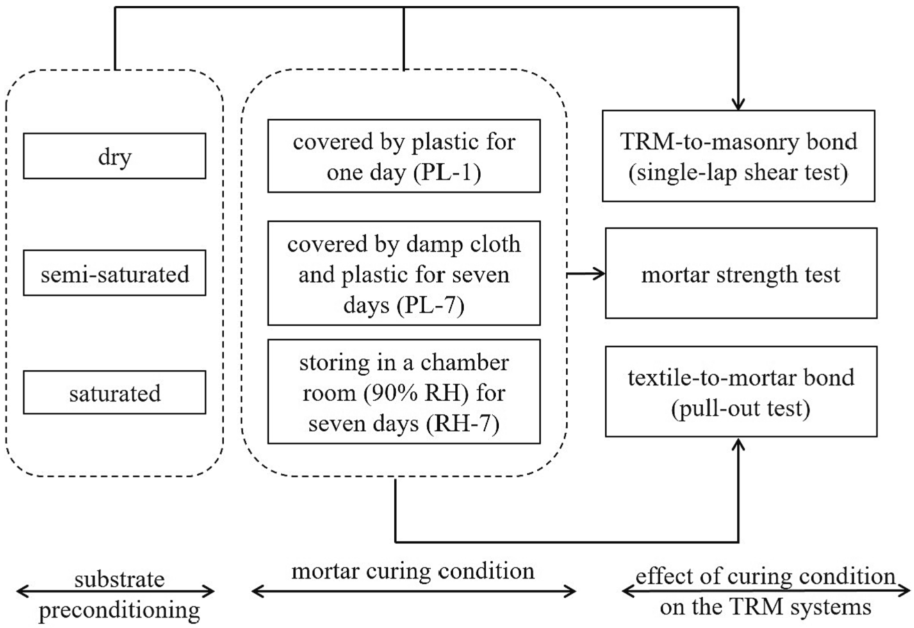

Fig. 1. General overview of the considered curing conditions.

mm^3 were used. Meanwhile, the specimens for flexural strength and elastic modulus measurements were prismatic (40 × 40 × 160 mm^3). The compressive and flexural strengths were characterized perpendicular to the flatwise direction of the brick, and the elastic modulus was measured only along the lengthwise direction. For each brick moisture condition (see Section 2.3) and type of tests, five specimens were used, leading to a total of 45 specimens (3 × 3 × 5).

The compressive and flexural tests were performed utilizing a Lloyd

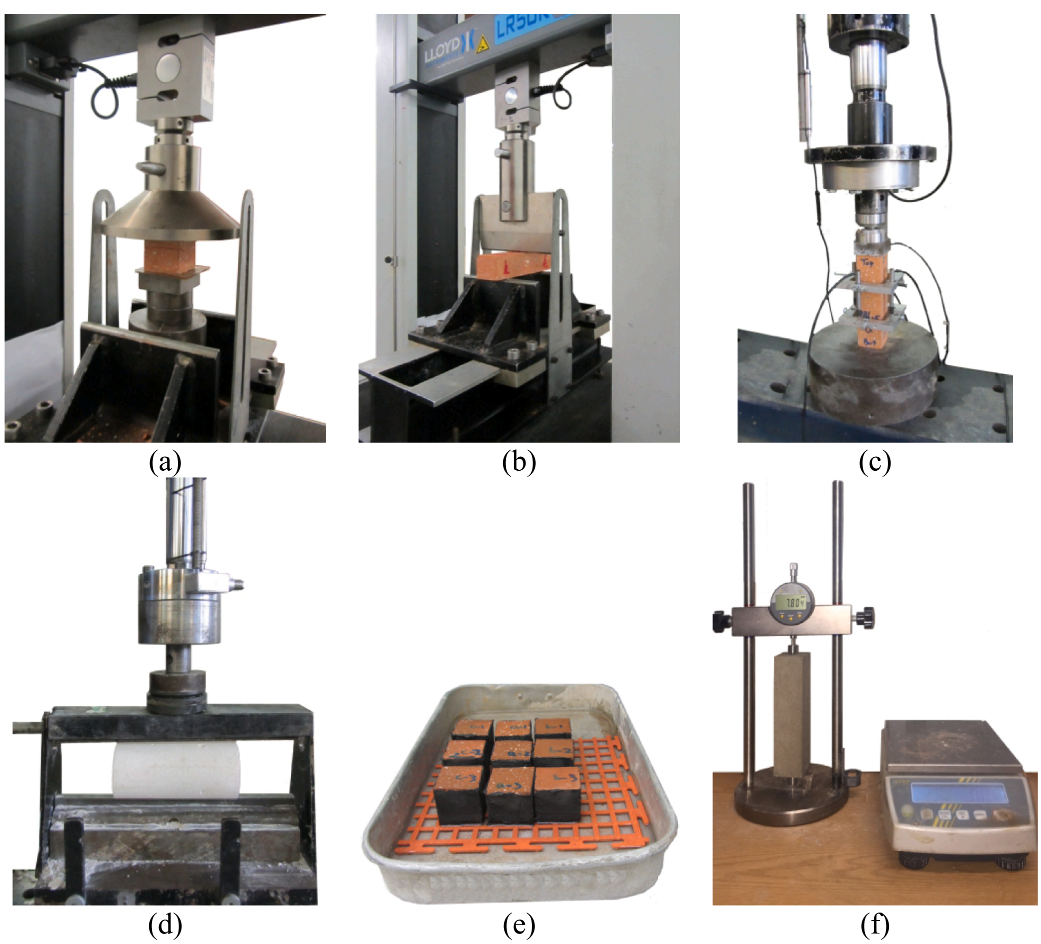

Fig. 2. Mechanical characterization tests: (a) compressive; (b) flexural; (c) elastic modulus; (d) splitting; (e) water absorption; (f) shrinkage test.

testing machine under force-controlled conditions at a rate of 150 N/s and 10 N/s, respectively. In the compressive tests, for reducing the friction, a pair of Teflon sheets (with a layer of oil in between) was placed between the specimen and the machine plates (Fig. 2a). The flexural tests were performed according to the three-point bending test scheme with a 100 mm distance between the supports (Fig. 2b). For measuring the elastic modulus, a universal testing machine (load capacity of 100 kN) equipped with LVDTs (3 for cylinder and 4 for prismatic specimens) with a 5 mm range and 1-μm sensitivity were used (Fig. 2c). Tensile splitting tests were performed using a universal testing machine and introducing monotonic displacements at a rate of 0.12 mm/min (Fig. 2d).

Water absorption characteristics of the mortar M2 and the brick were also investigated. The specimens included cubes of mortar with dimensions of 50 × 50 × 50 mm^3 and of brick with dimensions of 40 × 40 × 40 mm^3. The original brick was used for this test. Since sandblasting makes the brick surface rougher, it impossible to calculate the net-area of the brick accurately, leading errors in the test results. The mortar specimens were cured under three different curing conditions as explained in Section 2.3 and tested after 60 days. Water absorption due to capillary action was tested according to BS EN 1015-18 [35]. For this purpose, four side faces of the specimens were sealed with silicon. Then, the specimens were dried in a ventilated oven at a temperature of 90 °C until reaching a constant mass. Finally, the specimens were immersed in water for a depth of 10 mm, as shown in Fig. 2e, and their weights were measured periodically. The initial rate absorption (IRA) of the brick was calculated from the capillary absorption tests (after one minute) and according to BS EN 772-11 [36].

The capillary water absorption of the bricks was investigated along three directions (flatwise, lengthwise, and widthwise directions). As the mortar is expected to be isotropic, the water absorption tests were only performed in one direction (perpendicular to the surface into which the mortar was poured). Three specimens were used for each curing condition and direction, and the average results are presented here.

The effect of curing conditions on the mortar shrinkage was also determined. For this aim, prismatic shape specimens (40 × 40 × 160 mm^3) were prepared with both mortars M1 and M2. Three specimen types were considered for shrinkage measurements. Type I and II specimens were cured under PL-1 (one day under a plastic sheet) and PL-7 (seven days covered by damp cloths and under a plastic sheet) conditions, respectively. Meanwhile, type III specimens were prepared with a layer of AR-glass fabric placed in the middle, including two warp yarns

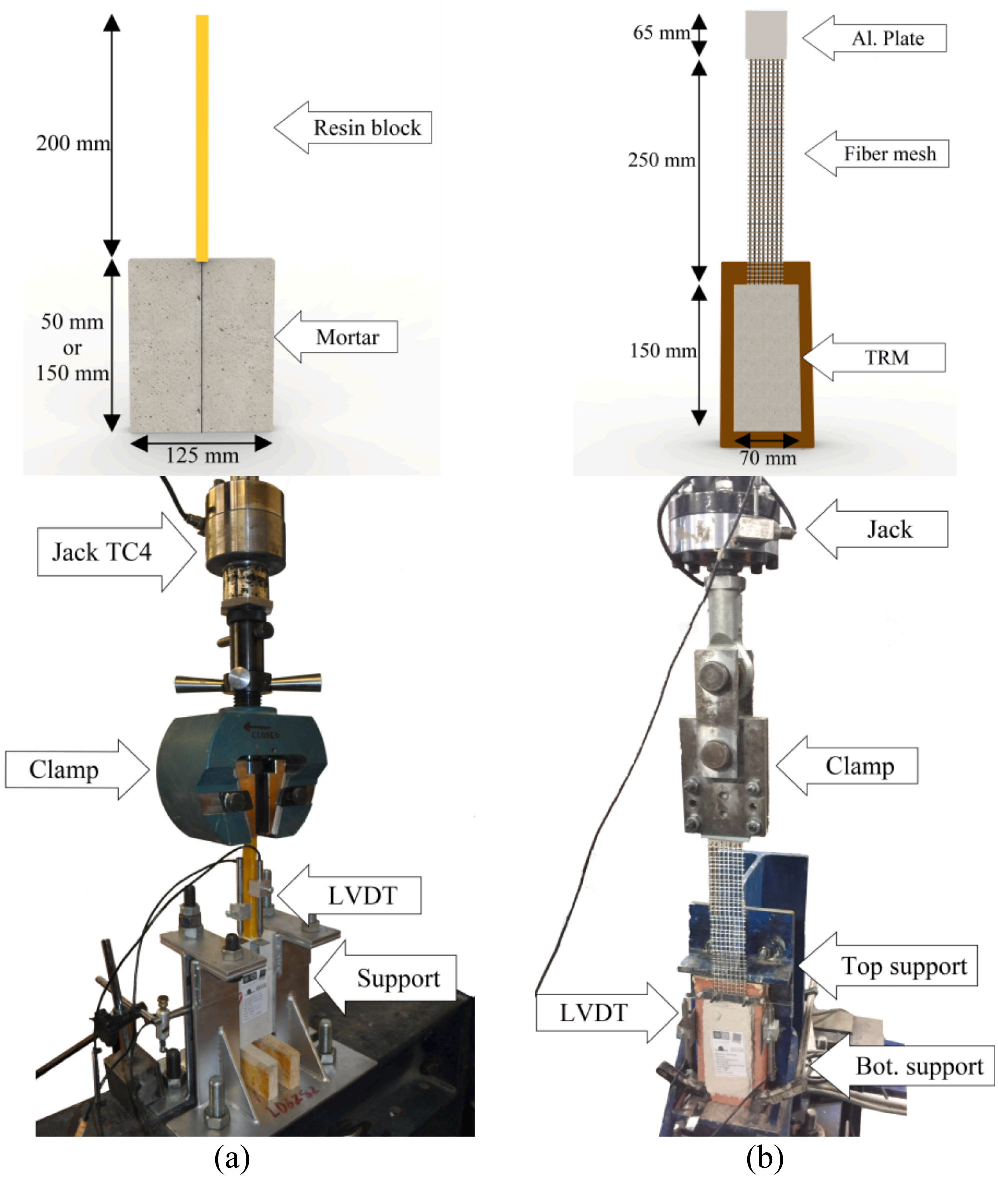

Fig. 3. Configuration and test setups: (a) pull-out test; (b) single-lap shear test.

and six weft yarns, and cured under the PL-7 conditions to understand the role of reinforcement on the shrinkage results. The specimens were demolded after two days, when the measurement of the shrinkage strains was initiated following EN 12617-04 [37], see Fig. 2f.

2.5. Pull-out tests

Pull-out tests were carried out on single cords/yarns embedded in mortar. The single steel cord and glass yarns were embedded in the mortars M2 and M1, respectively. For the preparation of the samples, firstly, single cord/yarns were embedded in an epoxy resin block over a 200 mm length and with a rectangular cross-sectional area of 10 × 16 mm^2. Then, the free length of the fiber was embedded in cuboid disk-shaped mortars with a cross-section of 125 × 16 mm^2 (Fig. 3a). The embedded length of the steel and the glass-based TRM were 150 mm and 50 mm, respectively, selected based on previous studies [4,13]. For further details on the procedure followed for the preparation of the pull-out specimens, please refer to [38]. The specimens were demolded after 24 h of preparation and then were cured in similar conditions as the mortar (as explained in Section 2.3). Five specimens were prepared for each curing condition and tested at 60 days (a total of 15 specimens, 3 × 5, for each TRM type studied).

The single-sided pull-out test setup developed and presented by the authors in [38] was used for examining the fiber-to-mortar bond performance. A U-shape steel support was used to support the specimens to a rigid frame for performing the pull-out tests. A mechanical clamp was gripped to the epoxy resin block (and thus the fiber) from the top. The tests were performed using a servo-hydraulic system with a maximum capacity of 25 kN by pulling the clamp at a displacement rate of 1.0 mm/min (Fig. 3a). Two LVDTs with a 20 mm range and 2-μm sensitivity located at both sides of the epoxy block recorded the slip. The average of these LVDT measurements is presented as the slip in the experimental results.

2.6. Single-lap shear tests

The bricks' largest surface (in a flatwise direction) was sandblasted before applying the TRM composite on the surface to improve the bond properties at the brick-to-mortar interface [39]. The sandblasting was performed three times at a speed of 800–900 m/s. Then the bricks were washed and cleaned with an air compressor to remove the dust.

Only the steel-based TRM was used for these tests. The mortar M2 was applied in two layers of 5 mm thickness and over an area of 150 mm × 70 mm, as shown in Fig. 3b. After applying the first layer of the mortar, the steel mesh (including eight longitudinal cords) was placed on the mortar, then the second layer of the mortar was applied. The embedded and free length of the fiber mesh was 150 mm and 250 mm, respectively (Fig. 3b). The specimens were cured following a similar procedure as the pull-out and the mortar specimens. Forty-eight hours before the testing, two aluminum plates were attached directly to the mesh extremity's free end to simplify the specimens' gripping during the tests and ensure a uniform transfer of the load to the fibers. Five specimens were prepared for each mortar curing condition and brick moisture conditions and tested at the age of 60 days (a total of 45 specimens, 3 × 3 × 5).

A closed-loop servo-controlled testing machine with a maximum load capacity of 50 kN at a displacement rate of 0.3 mm/min was used for performing the tests. A stiff supporting frame and two clamps held the specimens, as shown in Fig. 3b. Two LVDTs with a 20 mm range and 2-μm sensitivity placed at the loaded end measured the slip of the TRM-to-substrate. A preload of 200 N was applied to specimens before testing to simplify the attachment of the LVDTs.

3. Experimental results and discussion

3.1. Material properties

3.1.1. Mortars

Fig. 4 shows DTA results of the mortar M2 at 1, 7, and 60 days. The curves present three different peak points: water evaporation (at 50–100 °C), dehydroxylation (losing chemically bound water of $Ca(OH)_2$ at 360 ~ 440 °C), and decarboxylation (losing chemically bound CO_2 of $CaCO_3$ at 600–850 °C) [40,41]. The DTA results illustrate that the specimens cured under PL-7 condition show the highest water evaporation at 1 and 7 days. This indicates that the internal moisture of the samples is maintained under the PL-7 conditions. Specimens cured under PL-7 and RH-7 conditions show a higher dehydroxylation level at seven days than those cured under PL-1 conditions. During the first seven days, more moisture was available in PL-7 and RH-7 conditions, leading to the advancement of the hydration reactions and forming more $Ca(OH)_2$ in those samples [42]. The level of dihydroxylation, however, becomes similar in all curing conditions at 60 days, indicating the hydration reactions have ceased. Decarboxylation level is higher in the specimens cured under PL-7 and RH-7 conditions than those cured under PL-1 conditions at all tested ages. This shows the presence of a higher $CaCO_3$ and carbonation degree in those samples. The increase of the decarboxylation peak (and so $CaCO_3$) at 60 days (Fig. 4c) is consistent with the reduction of the dehydroxylation peak and $Ca(OH)_2$ showing achievement of a higher level of carbonation in those samples.

The mean strength (compressive, flexural, and splitting) of the mortars M1 and M2 cured under different conditions are presented in Table 3. The results indicate that conservation of the moisture at early ages leads to the achievement of higher mechanical properties, as expected. The enhancement of the mechanical properties is more significant in mortar M1 (e.g. a 31 % and 47 % higher strength is observed under PL-7 and RH-7 conditions, respectively, compared to PL-1 conditions), than in mortar M2 (in which the enhancement of the strength was 8 % and 9 %).

The effect of curing conditions on the pore structure (porosity, connectivity and tortuosity) of the mortars can also be indirectly investigated from the water absorption test results Table 3. The capillary coefficient of the mortar M2 cured under PL-1 conditions is higher than that of the specimens cured under high humidity conditions (PL-7 and RH-7), showing that those mortars have a more porous and connected microstructure [43].

Fig. 5 and Table 3 show the average shrinkage and variation of the weight of the specimens during the tests. The effect of glass fabric and steel mesh fiber on the mortar shrinkage strain is notable. The reinforced mortars M1 and M2 (PL-7_reinforced in Fig. 5a, b) show 12 % and 24 % less shrinkage than the unreinforced specimens cured under similar conditions (PL-7) [44].

The effect of curing conditions on the shrinkage strain of the mortars is also significant. M1 specimens cured under PL-7 conditions shrink twice of those cured under PL-1 conditions, while this value is 38 % in M2 specimens. A higher humidity at an early age can be the reason for this difference between the results of PL-7 and PL-1. This observation can be attributed to the fact that higher humidity in the early ages promotes a higher degree of hydration and carbonation reactions [45,46]. Furthermore, since the mortar M1 consists of pozzolan, higher humidity causes the pozzolanic reactions to accelerate and consume more moisture within the mortar, resulting in higher shrinkage [47]. Those curing conditions also ensure a higher initial moisture content in the samples; hence a higher drying shrinkage is observed. Further investigation is necessary to determine how hydration, carbonation, and pozzolanic reactions contribute to shrinkage.

3.1.2. Brick

Table 4 shows the mechanical properties of the clay brick. The effect of water content on the mechanical properties of the brick is significant.

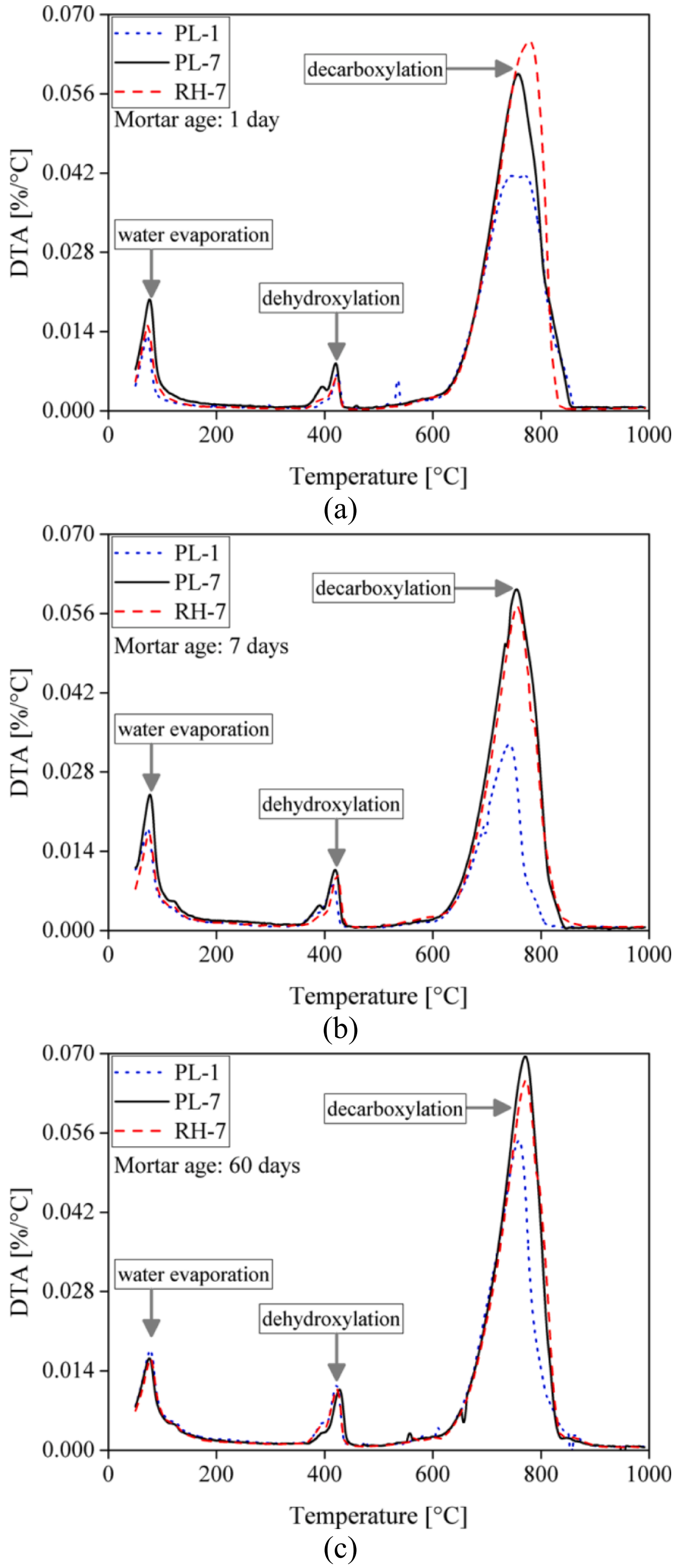

Fig. 4. Differential thermal analyses (DTA) results of mortar M2 at: (a) 1 day; (b) 7 days; (c) 60 days.

Table 3
Mortar mechanical and physical properties at 60 days*.

Test	Mortar	Curing conditions		
		PL-1	PL-7	RH-7
Compressive strength [MPa]	M1	6.70 (14)	8.79 (12)	9.82 (2)
	M2	6.89 (6)	7.47 (5)	7.51 (14)
Flexural strength [MPa]	M1	4.07 (5)	5.20 (12)	5.22 (5)
	M2	1.68 (6)	1.78 (10)	2.08 (5)
Elastic modulus [MPa]	M1	6265 (11)	7177 (9)	8038 (5)
	M2	8759 (8)	9216 (6)	9748 (6)
Splitting tensile strength [MPa]	M1	0.93 (9)	1.16 (8)	1.33 (7)
	M2	0.39 (18)	0.71 (23)	1.12 (9)
Capillary coefficient [kg/(m^2 × min$^{0.5}$)]	M2	0.45 (10)	0.37 (11)	0.38 (8)
Shrinkage strain	M1	0.14 (15)	0.28 (7)	–
	M2	0.17 (2)	0.21 (8)	–

*Coefficients of variation in percentage terms are provided inside parentheses. PL-1: curing under plastic for one day; PL-7: curing under plastic and covered with damp cloths for 7 days; RH-7: curing inside a chamber room with 90 % RH.

The semi and saturated bricks show a 7 % and 27 % reduction of strength compared to the dry bricks. This reduction is 7 % and 11 % for the flexural strength. These observations show that by increasing the moisture content of the brick, its strength decreases. However, the elastic modulus remains constant by considering variation.

Table 4 also presents the IRA and the water absorption coefficients of the brick. The IRA coefficient is the lowest for the flatwise direction of the brick and the highest for the widthwise direction. This means that if the fresh mortar is applied on the widthwise surface of the brick, the moisture will transfer from the mortar to the brick rapidly. However, applying mortar on the brick's flatwise surface (with low IRA), as it is usually done in single-lap shear tests and as opposed to what happens in practice, causes the bricks to absorb less water from mortar [25,26] hence affecting the final bond performance. The capillary absorption coefficient of the brick in the flatwise direction also supports this observation, where its coefficient is less over a longer period than the other directions (Table 4). It should be considered in reality TRM composites are applied on masonry consisting of bricks (lengthwise) and mortar and therefore more realistic results can be achieved when bond tests are performed on masonry prisms rather than bricks. However, the bond between TRMs and the brick substrates are as important as, if not more, the bond between TRM and mortar joints. The results from the capillary absorption tests, Fig. 6, show the brick's moisture content reaches 60 % saturation degree after 165 min of capillary tests along the flatwise direction. This period is therefore chosen for semi saturation of the bricks in single-lap shear bond tests.

3.2. *Pull-out test results*

3.2.1. *Steel reinforced mortar*

All steel-based TRM specimens failed due to fibers slippage from the mortar, resulting in typical load-slip curves presented in Fig. 7. The pull-out curves show a sudden drop in the load to a residual value P_f after reaching the peak load (P_P) due to the occurrence of debonding between

Table 4
Brick properties*.

Mechanical tests	Brick conditions		
	Dry	Semi saturated	Saturated
Compressive strength [MPa]	25.2 (2)	23.5 (5)	18.4 (6)
Flexural strength [MPa]	5.5 (1)	5.1 (9)	4.9 (13)
Elastic modulus [MPa]	10,660 (5)	10,363 (4)	10,328 (2)
Physical tests	Test direction		
	flatwise	lengthwise	widthwise
IRA [kg/(m^2 × min)]	0.47 (9)	0.79 (2)	1.03 (5)
Capillary coefficient [kg/(m^2 × min$^{0.5}$)]	0.32 (1)	0.59 (2)	0.61 (8)

*Coefficients of variation in percentage terms are provided inside parentheses.

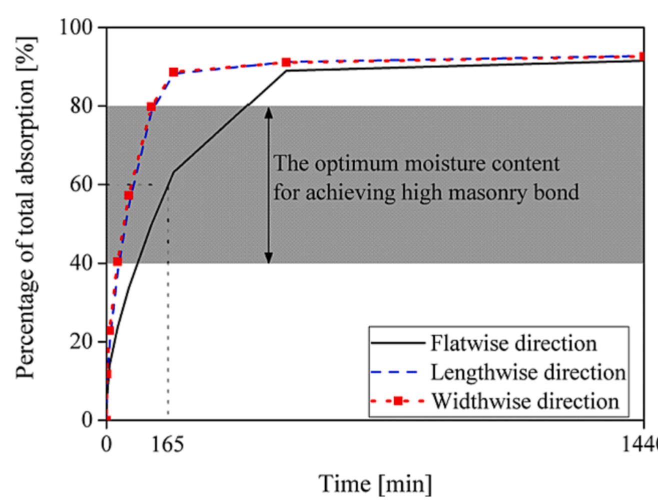

Fig. 6. The ratio of capillary moisture content of the brick to the total absorption as a function of time.

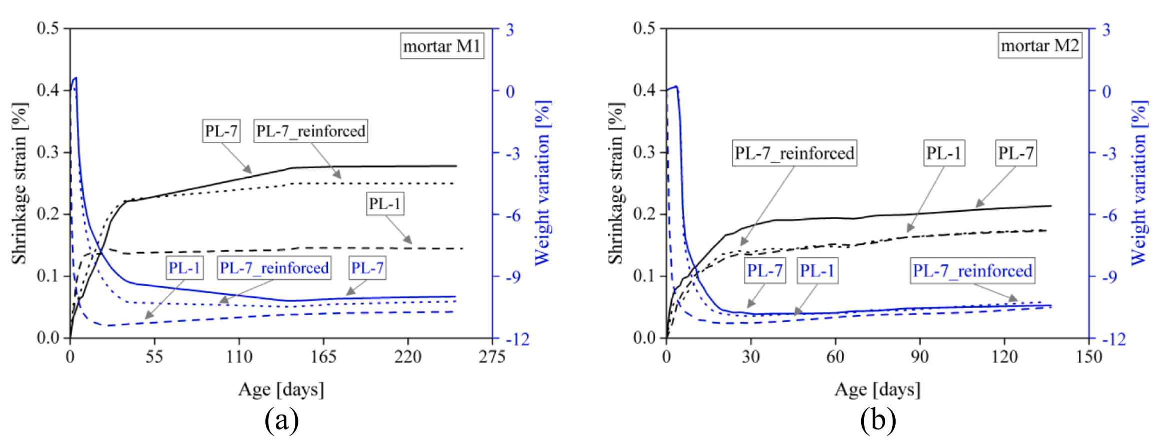

Fig. 5. Shrinkage strain and weight changes under different curing conditions: (a) mortar M1; (b) mortar M2.

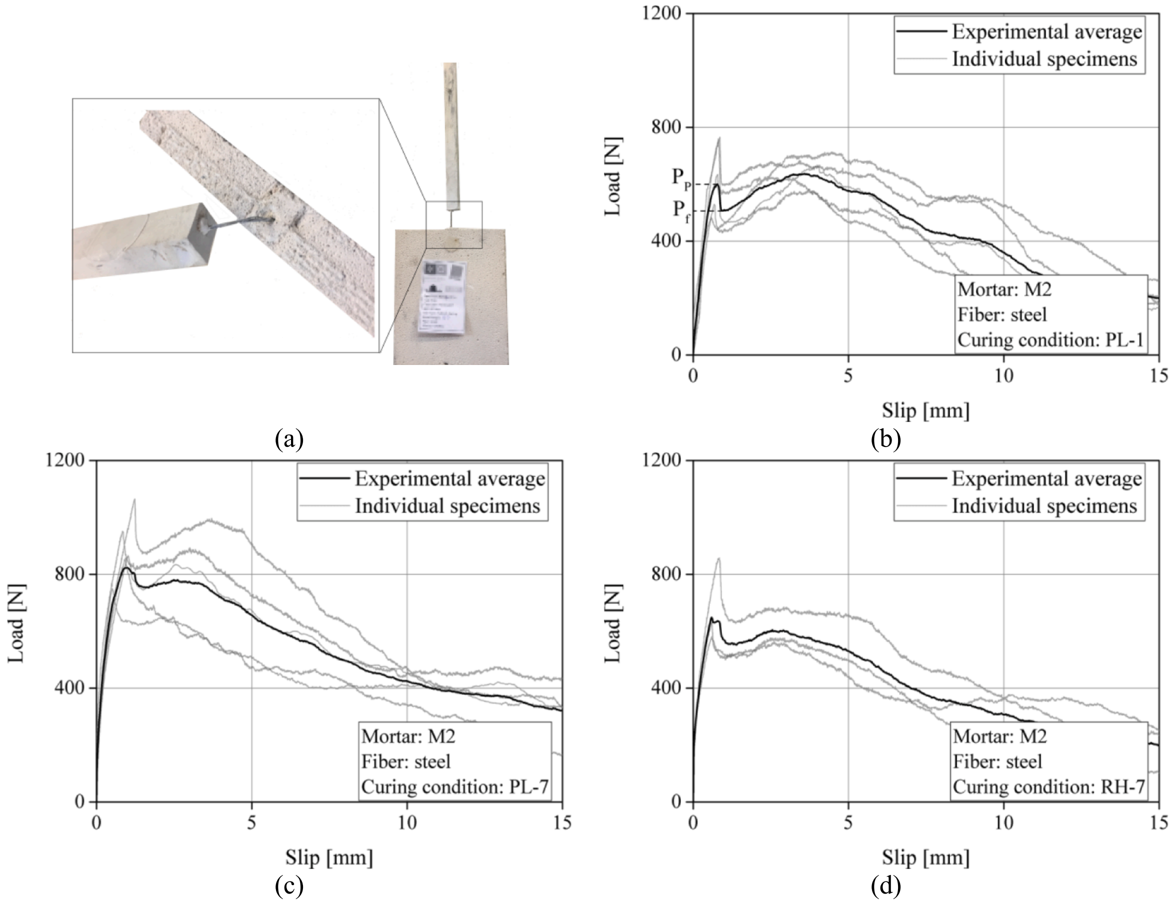

Fig. 7. Typical failure mode and pull-out load-slip curves of steel-based TRM specimens: (a) fiber slippage; (b) P_PL-1_St; (c) P_PL-7_St; (d) P_RH-7_St.

the fiber and the mortar [48], as shown in Fig. 7a. A slip hardening behavior follows this sudden drop by reaching the second peak load, resulting from friction between the fiber and the mortar. Comparison of average load-slip curves (Fig. 7b–d) reveals that slip hardening is smaller in samples cured under PL-7 and RH-7 conditions compared to samples cured under PL-1 conditions. Nevertheless, the curing conditions considered here do not affect the general form of the load-slip curves.

Table 5 presents the main characteristics of the experimental pull-out curves and analytically obtained bond-slip laws (see [38,48] for analytical calculations) for each curing condition. The pull-out parameters include the first peak load (P_P), the dropped load (P_f), the initial stiffness (K), the debonding energy (E_{deb}), and the pull-out energy (E_{po}). E_{deb} and E_{po} are the areas under the load-slip curve until the P_P and from the P_P until the end, respectively. The bond-slip law parameters include bond shear strength (τ_{max}), frictional shear strength (τ_f), and bond modulus (κ), as presented in Fig. 8.

In general, the specimens cured under PL-7 and RH-7 show a much better bond performance than specimens cured under PL-1, as shown in Table 5. The P_P, K, and E_{deb} of the P_PL-7_St specimens, which explain the fiber-to-mortar bond behavior before full debonding, are 41 %, 168 %, and 120 %, respectively higher than those of P_PL-1_St specimens are. These values are also 9 %, 112 %, and 15 % higher in the P_RH-7_St specimens compared to P_PL-1_St specimens. This translates to 119 %

Table 5
Effect of curing conditions on the textile-to-mortar bond properties*.

TRM composite	Specimen	P_P [N]	P_f [N]	K [N/mm]	E_{deb} [N.mm]	E_{po} [N.mm]	τ_{max} [MPa]	τ_f [MPa]	κ [N/mm^3]
Steel-based TRM	P_PL-1_St	635	500	1190	290	6093	2.21	1.28	6.17
		(18)	(14)	(14)	(29)	(15)	(19)	(14)	(26)
	P_PL-7_St	898	763	3194	639	7534	4.83	1.93	46.92
		(12)	(12)	(5)	(19)	(15)	(10)	(13)	(9)
	P_RH-7_St	689	544	2528	334	5720	3.81	1.41	26.54
		(18)	(11)	(4)	(33)	(14)	(24)	(12)	(15)
Glass-based TRM	P_PL-1_Gl	153	133	857	19	3848	1.17	0.81	2.61
		(18)	(22)	(11)	(26)	(6)	(8)	(17)	(33)
	P_PL-7_Gl	187	193	1107	27	4433	1.18	1.02	13.02
		(12)	(9)	(12)	(12)	(11)	(4)	(9)	(9)
	P_RH-7_Gl	208	197	1042	71	3714	2.43	0.97	32.21
		(11)	(2)	(8)	(19)	(8)	(8)	(18)	(20)

*Coefficients of variation in percentage terms are provided inside parentheses.

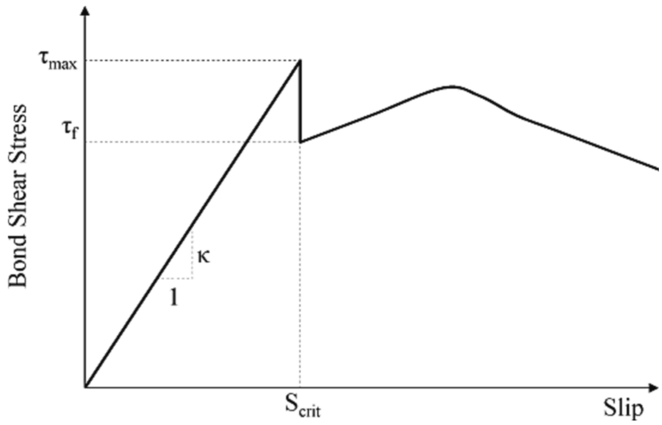

Fig. 8. Bond shear stress-slip law [38,48].

and 72 % higher bond strength (τ_{max}) and 660 % and 330 % higher bond modulus (κ) in the P_PL-7_St and P_RH-7_St specimens compared to the P_PL-1_St specimens. The τ_f is also 51 % and 10 % higher in P_PL-7_St and P_RH-7_St specimens. These findings suggest that increased humidity at the early age of mortar improves the fiber-to-mortar bond behavior. These observations are also in line with the changes in the strength of mortar M2 under different curing conditions (Table 3).

Comparing P_PL-7_St and P_RH-7_St, it is evident that conserving moisture with plastic leads to a higher bond performance than curing under high humidity conditions, see Table 5. For example, the P_P, τ_{max}, and τ_f of P_PL-7_St specimens are 30 %, 27 %, and 37 %, respectively, higher than those of P_RH-7_St. Although the mechanical strength of mortar M2 cured under these two curing conditions is similar (see Table 3), the DTA results showed that the decarboxylation level of the specimens cured under the PL-7 conditions is higher than those cured under RH-7 conditions. This indicates a higher carbonation degree achieved in those samples, which leads to better bond performance.

3.2.2. *Glass-reinforced mortar*

The yarn slippage was the main failure mode of the glass-based TRM composites for all three curing conditions, as presented in Fig. 9. The average and individual load-slip curves for these specimens under different curing conditions are also shown in Fig. 9. Like the steel-based TRM, the experimental results show the typical pull-out curves.

Similarly, the conservation of moisture in early ages has a considerable contribution to the glass-to-mortar bond behavior. As reported in Table 5, P_P, K, and E_{deb} of the P_PL-7_Gl specimens are 22 %, 29 %, and 42 % higher than the P_PL-1_Gl specimens. These values are 36 %, 22 %, and 274 % higher in the P_RH-7_Gl specimens than the P_PL-1_Gl specimens. The other bond parameters also show a similar enhancement in the P_PL-7_Gl and P_RH-7_Gl specimens compared to the P_PL-1_Gl specimens. This could be attributed to the role of moisture in the enhancement of the hydration and bond formation at the textile-to-mortar interface. Higher shrinkage observed in PL-7 specimens compared to PL-1 samples (Fig. 5a) can also lead to further confinement of the fabric and, therefore, enhancement of the frictional bond, τ_f, and its bond modulus (κ), as presented in Table 5. A comparison of P_PL-7_Gl and P_RH-7_Gl bond parameters indicates that PL-7 (curing seven days under wet clothes and plastic) and RH-7 (curing seven days in chamber room with 90 % RH) conditions have the same effect on the glass-based TRM pull-out.

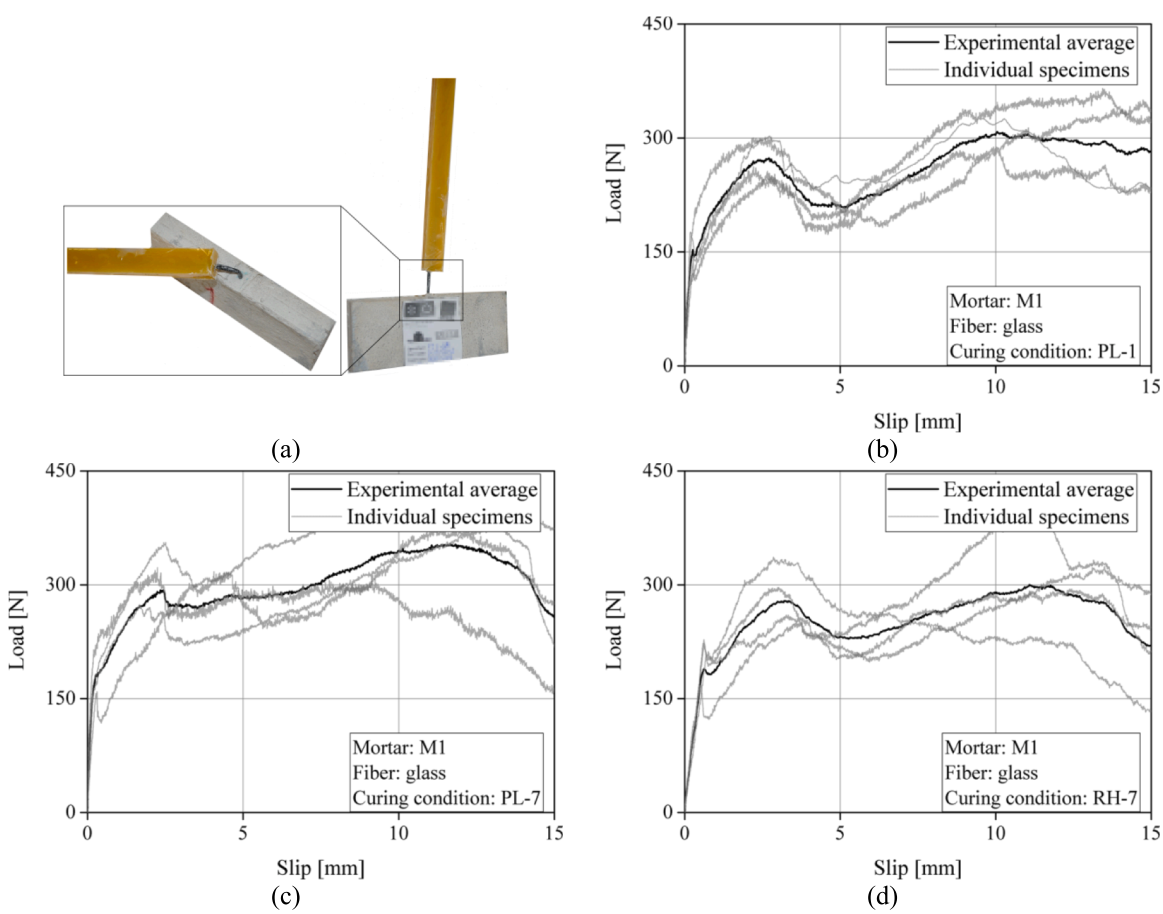

Fig. 9. Typical failure mode and pull-out load-slip curves of glass-based TRM specimens: (a) yarn slippage; (b) P_PL-1_Gl; (c) P_PL-7_Gl; (d) P_RH-7_Gl.

3.3. Single-lap shear test results

The main outputs of single-lap shear tests (load-slip curves, peak load (P_P), bond strength (σ_P), and failure mode of the specimens) are presented and discussed in this section. Here, the bond strength is calculated by dividing the peak load by the fiber cross-section area. The ratio of the bond strength to the tensile strength of steel cord (η) is also presented to investigate the effect of different curing conditions on the utilization of the tensile strength in the TRM systems.

3.3.1. Dry substrate

Fig. 10a–c and Table 6 show the load-slip curves and the summary of the S_PL-1_D, S_PL-7_D, and S_RH-7_D test results. The load-slip curves show a similar trend in all specimens comprising an elastic stage followed by a short nonlinear stage (see Fig. 10a–c). Debonding at the TRM-to-substrate interface was the main failure mode of all the tested specimens (see failures in Fig. 11a–c). This shows that the bond between the TRM and the substrate is weaker than the bond at the fiber-to-mortar interface in these specimens. Although the surface of the bricks was sandblasted to improve the mortar-to-substrate bond [39], using dry bricks led to a poor bond performance because of the suction of the mortar water towards the brick [49,50].

Interestingly, the specimens cured under PL-7 conditions (S_PL-7_D) show a lower peak load (P_P) than the specimens cured under the other conditions (S_PL-1_D and S_RH-7_D), as listed in Table 6. This observation contrasts with the pull-out results. This shows high drying shrinkage in those specimens, as discussed in Section 3.1.1, has possibly led to the development of micro-cracks at the mortar-to-brick surface and reduction of its bond performance.

3.3.2. Semi-saturated substrate

These specimens showed a ductile load-slip curve (deformation ability after reaching the peak load), see Fig. 10d–f. As opposed to the specimens prepared on dry substrate, the failure of all these specimens was fiber slippage followed by mortar cracking (Fig. 11d–f) in these specimens. This indicates a better bond is formed between the mortar and the brick, in this case [2,25,51,52].

A comparison between the bond parameters of this group of specimens shows that S_PL-7_SS specimens have a better performance than two other series (Table 6). This can be due to the presence of sufficient moisture in these specimens, thus improving the fiber-to-mortar bond in a similar way to pull-out specimens (P_PL-7_S). Also, it seems that the bond performance in the specimens cured under high relative humidity conditions (P_RH_7_SS) does not differ much from the specimens cured under plastic for one day (P_PL_1_SS).

Table 6
Effect of curing conditions on the TRM-to-brick bond properties*.

Brick moisture condition	Specimen	P_P [N]$_{per\ fiber}$	σ_P [MPa]	η [%]	Failure
Dry	S_PL-1_D	558 (8)	1037	35	A
	S_PL-7_D	365 (17)	678	23	A
	S_RH-7_D	652 (18)	1212	41	A
Semi-saturated	S_PL-1_SS	762 (17)	1416	48	B
	S_PL-7_SS	875 (8)	1626	55	B
	S_RH-7_SS	642 (9)	1193	38	B
Saturated	S_PL-1_SA	942 (4)	1751	59	B-C
	S_PL-7_SA	841 (17)	1563	53	B-C
	S_RH-7_SA	657 (18)	1221	41	B-C

*Coefficients of variation in percentage terms are provided inside parentheses; P_P: peak load; σ_P: maximum bond strength; η: maximum bond strength (σ_P) to the tensile strength of steel cord (2972 MPa). Failure A: debonding at the interface between TRM and substrate; Failure B: fiber slipping followed by mortar cracking; Failure C: fiber slipping followed by detachment at the fiber-to-mortar interface.

3.3.3. Saturated substrate

Fig. 10g–i shows the load-slip curves of the S_PL-1_SA, S_PL-7_SA, S_RH-7_SA specimens. Compared with the dry bricks, these specimens demonstrate a higher ductility and bond strength. However, their load-slip curves lack the post-peak region observed in specimens prepared on semi-saturated bricks due to the type of failure mode that occurred in these specimens (combined fiber slipping and mortar cracking followed by detachment at the fiber-to-mortar interface, Fig. 11g–i). As shown in Table 6, the S_PL-1_SA specimens have a better bond performance than the S_PL-7_SA and S_RH-7_SA specimens. This improvement in the bond behavior can be attributed to the water balance within the mortar during curing condition PL-1. It seems that the presence of high humidity (in PL-7 and RH-7) combined with a saturated substrate has not resulted in a reduction in the moisture content of the mortar, thus increasing its potential for shrinkage [53]. This observation can also be supported with the shrinkage characteristic of the mortar presented in Section 3.1.1, where higher humidity can affect its shrinkage behavior.

A comparison between saturated and dry bricks shows an increase in the bond strength. According to Table 6, the η for the specimens prepared on saturated bricks is in the range of 41 % to 59 %. In contrast, this range falls between 23 % and 41 % for dry brick samples. Thus, the higher moisture content of the brick, the higher bond strength.

3.3.4. Interaction of mortar curing and brick moisture conditions

The brick condition appears to have a significant impact on the TRM-to-substrate bond behavior. Comparing the exploitation ratio (η) of the samples S_PL-1_D, S_PL-1_SS, and S_PL-1_SA (dry, semi-, and saturated bricks with mortar curing condition PL-1), η has increased when the bricks have a higher initial moisture content (η = 35 %, 48 %, and 59 %, respectively). However, curing the mortar under high humidity conditions during the early ages (curing PL-7 and RH-7 in this study) can reduce the effect of substrate conditions on the bond performance. These findings are also corroborated by comparing the peak loads (P_P) of the pull-out and the single-lap shear tests. Under PL-1 curing conditions and semi-saturated or saturated substrate conditions (SS and SA conditions), the P_P of the single-lap shear tests is more than that of the pull-out test. For PL-7 conditions, the P_P of the pull-out and single-lap shear tests are in the same range (however, the P_P is smaller for the dry brick condition). Comparable results are also observed for RH-7 conditions. As a result, it is clear that the high moisture content in the mortar (due to either proper curing or lack of suction of mortar water by the substrate) results in a higher degree of hydration in the mortar and a better the bond performance.

4. Conclusions

An experimental investigation on the effect of preconditioning and curing on the bond performance of two conventional TRM composites used to strengthen masonry substrates (fiber-to-mortar and TRM-to-substrate bond performance) was presented in this study. Three substrate moisture conditions and three different curing conditions were considered for this purpose. From the obtained results, the following main conclusions can be drawn:

- The mechanical and physical characterization tests performed on constituent materials showed the importance of curing conditions on the development of mechanical properties and pore structure of lime-based mortars. Although this importance varied in the two mortars studies here, overall, the mechanical properties were improved when the samples were cured under higher humidity conditions (either under plastic or in high humidity rooms). The drying shrinkage, again dependent on the type of mortar, was also higher in specimens

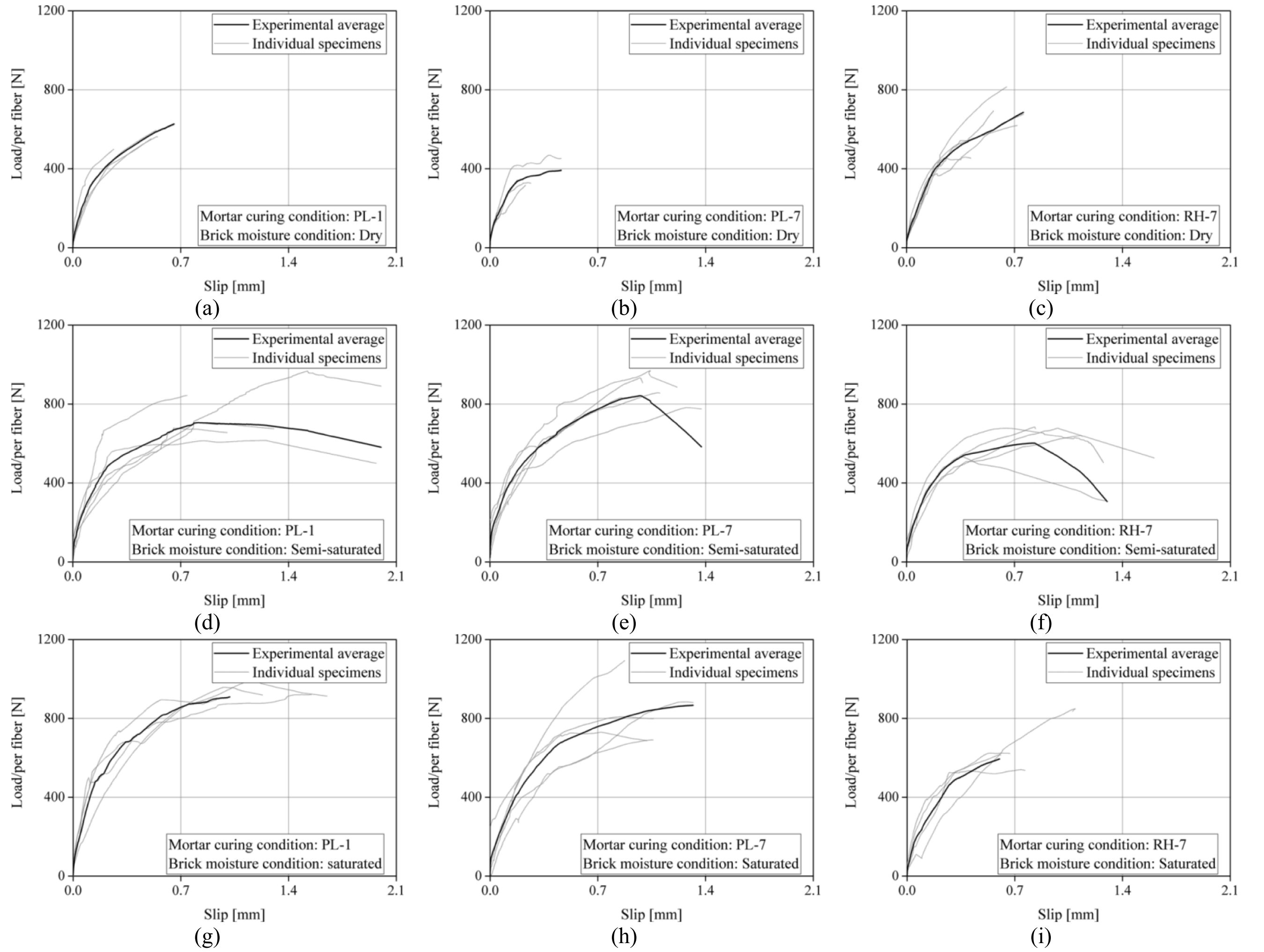

Fig. 10. Single-lap shear tests results: (a) S_PL-1_D; (b) S_PL-7_D; (c) S_RH-7_D; (d) S_PL-1_SS; (e) S_PL-7_SS; (f) S_RH-7_SS; (g) S_PL-1_SA; (h) S_PL-7_SA; (i) S_RH-7_SA.

cured under plastic for seven days compared to those cured for only one day.

- It was observed that extruded solid clay bricks show direction-dependent mechanical and transport properties. The capillary absorption coefficient and moisture absorption rate of the bricks in the widthwise direction was highest. This indicates that when fresh mortar is applied on the flatwise of the brick's surface (as is done in single-lap shear tests on TRM-strengthened bricks), the brick absorbs less water from the mortar compared to when it is applied on its widthwise or lengthwise directions (as is the case in real practice). The final bond performance will therefore be different, hence, questioning the suitability of single-lap shear tests when single bricks are used as the substrate.
- Curing conditions had a significant effect on the development of mechanical properties of mortar and the fiber-to-mortar bond behavior. The pull-out response of both steel- and glass-based TRMs was enhanced when the specimens were cured under high humidity conditions (RH-7) or under plastic (PL-7) for seven days compared to when those were cured under the plastic only for one day (PL-1). However, the curing conditions considered did not affect the overall shape of the load-slip curves or the failure mode of the specimens.
- It was observed that the initial water content of the substrate is the most critical parameter on the TRM-to-substrate bond behavior. Dry substrates absorbed water from the mortar and disrupted the chemical reactions of the mortar. Consequently, a poor bond between the mortar and the brick was formed; hence, the single-lap shear test samples failed by debonding at the TRM-to-substrate interface. Nevertheless, semi- or full saturation of the bricks led to the formation of a strong bond.
- The results show that TRM composites show better performance if the masonry substrate is properly conditioned before application. Covering the mortar surface with damp cloths and storing it under plastic for seven days (PL-7 condition) is helpful for hydraulic lime-based TRM composites.
- The results also show the importance of considering the substrate preparation and curing conditions when comparing the experimental results of TRM-masonry systems taken from different databases. These findings are crucial for standardization.

CRediT authorship contribution statement

Ali Dalalbashi: Investigation, Methodology, Formal analysis, Writing – original draft, Visualization. **Bahman Ghiassi:** Writing – review & editing, Supervision. **Daniel V. Oliveira:** Writing – review & editing, Supervision.

Declaration of Competing Interest

The authors declare that they have no known competing financial interests or personal relationships that could have appeared to influence

Fig. 11. Failure of the single-lap shear test samples: (a) S_PL-1_D; (b) S_PL-7_D; (c) S_RH-7_D; (d) S_PL-1_SS; (e) S_PL-7_SS; (f) S_RH-7_SS; (g) S_PL-1_SA; (h) S_PL-7_SA; (i) S_RH-7_SA.

the work reported in this paper.

Acknowledgements

FEDER funds partly funded this work through the Competitively Factors Operational Program (COMPETE) and by national funds through the Foundation for Science and Technology (FCT) within the scope of the project POCI-01-0145-FEDER-007633. The support to the first author through grant SFRH/BD/131282/2017 is gratefully acknowledged. The authors would like to thank the Kerakoll Company for supplying the GeoCalce Fino mortar and GeoSteel G600 fibers.

References

[1] W. Brameshuber (Ed.), RILEM TC 201-TRC: Textile Reinforced Concrete- State-of-the-art, RILEM, Bagneux, 2006.
[2] S. Barr, W.J. McCarter, B. Suryanto, Bond-strength performance of hydraulic lime and natural cement mortared sandstone masonry, Constr. Build. Mater. 84 (2015) 128–135, https://doi.org/10.1016/j.conbuildmat.2015.03.016.
[3] J. Lanas, J.L. Perez Bernal, M.A. Bello, J.I. Alvarez, Mechanical properties of masonry repair dolomitic lime-based mortars, Cem. Concr. Res. 36 (2006) 951–960, https://doi.org/10.1016/j.cemconres.2005.10.004.
[4] A. Dalalbashi, B. Ghiassi, D.V. Oliveira, A. Freitas, Fiber-to-mortar bond behavior in TRM composites: effect of embedded length and fiber configuration, Compos. B Eng. 152 (2018) 43–57, https://doi.org/10.1016/j.compositesb.2018.06.014.
[5] A. Razavizadeh, B. Ghiassi, D.V. Oliveira, Bond behavior of SRG-strengthened masonry units: testing and numerical modeling, Constr. Build. Mater. 64 (2014) 387–397, https://doi.org/10.1016/j.conbuildmat.2014.04.070.
[6] L. Ascione, G. De Felice, S. De Santis, A qualification method for externally bonded Fibre Reinforced Cementitious Matrix (FRCM) strengthening systems, Compos. B Eng. 78 (2015) 497–506, https://doi.org/10.1016/j.compositesb.2015.03.079.
[7] B. Ghiassi, D.V. Oliveira, V. Marques, E. Soares, H. Maljaee, Multi-level characterization of steel reinforced mortars for strengthening of masonry structures, Mater. Des. 110 (2016) 903–913, https://doi.org/10.1016/j.matdes.2016.08.034.
[8] A. Bilotta, F. Ceroni, E. Nigro, M. Pecce, Experimental tests on FRCM strengthening systems for tuff masonry elements, Constr. Build. Mater. 138 (2017) 114–133, https://doi.org/10.1016/j.conbuildmat.2017.01.124.
[9] S. De Santis, F. Ceroni, G. de Felice, M. Fagone, B. Ghiassi, A. Kwiecień, G. P. Lignola, M. Morganti, M. Santandrea, M.R. Valluzzi, A. Viskovic, Round robin test on tensile and bond behaviour of Steel Reinforced Grout systems, Compos. B Eng. 127 (2017) 100–120, https://doi.org/10.1016/j.compositesb.2017.03.052.
[10] S. De Santis, G. de Felice, Steel reinforced grout systems for the strengthening of masonry structures, Compos. Struct. 134 (2015) 533–548, https://doi.org/10.1016/j.compstruct.2015.08.094.
[11] E. Franzoni, C. Gentilini, M. Santandrea, S. Zanotto, C. Carloni, Durability of steel FRCM-masonry joints: effect of water and salt crystallization, Mater. Struct. 50 (2017) 1–16, https://doi.org/10.1617/s11527-017-1070-2.
[12] A. Dalalbashi, S. De Santis, B. Ghiassi, D.V. Oliveira, Slip rate effects and cyclic behaviour of textile-to-matrix bond in textile reinforced mortar composites, Mater. Struct. 54 (2021), https://doi.org/10.1617/s11527-021-01706-w.
[13] A. Dalalbashi, B. Ghiassi, D.V. Oliveira, Textile-to-mortar bond behaviour in lime-based textile reinforced mortars, Constr. Build. Mater. 227 (2019), 116682, https://doi.org/10.1016/j.conbuildmat.2019.116682.
[14] S. Reichenbach, P. Preinstorfer, M. Hammerl, B. Kromoser, A review on embedded fibre-reinforced polymer reinforcement in structural concrete in Europe, Constr. Build. Mater. 307 (2021), 124946, https://doi.org/10.1016/j.conbuildmat.2021.124946.
[15] X. Wang, C.C. Lam, V.P. Iu, Bond behaviour of steel-TRM composites for strengthening masonry elements: experimental testing and numerical modelling, Constr. Build. Mater. 253 (2020), 119157, https://doi.org/10.1016/j.conbuildmat.2020.119157.
[16] N. Trochoutsou, M. Di Benedetti, K. Pilakoutas, M. Guadagnini, Bond of flax textile-reinforced mortars to masonry, Constr. Build. Mater. 284 (2021), 122849, https://doi.org/10.1016/j.conbuildmat.2021.122849.
[17] S.M. Raoof, L.N. Koutas, D.A. Bournas, Bond between textile-reinforced mortar (TRM) and concrete substrates: Experimental investigation, Compos. B Eng. 98 (2016) 350–361.
[18] A. Bellini M. Antonietta Aiello F. Bencardino B. de Carvalho Bello G. Castori A. Cecchi F. Ceroni M. Corradi T. D'antino S. De Santis M. Fagone G. de Felice M. Leone G.P. Lignola A. Napoli M. Nisticò C. Poggi A. Prota G. Ranocchiai R. Realfonzo E. Sacco C. Mazzotti Influence of different set-up parameters on the bond behavior of FRCM composites Construction and Building Materials. SP-345 (2021) 185 195 10.1016/j.conbuildmat.2021.124964.
[19] C. Caggegi, D. Sciuto, M. Cuomo, Experimental study on effective bond length of basalt textile reinforced mortar strengthening system: Contributions of digital image correlation, Measure. J. Int. Measure. Confed. 129 (2018) 119–127, https://doi.org/10.1016/j.measurement.2018.07.003.
[20] G. de Felice, M.A. Aiello, A. Bellini, F. Ceroni, S. De Santis, E. Garbin, M. Leone, G. P. Lignola, M. Malena, C. Mazzotti, M. Panizza, M.R. Valluzzi, Experimental characterization of composite-to-brick masonry shear bond, Mater. Struct. 49 (7) (2016) 2581–2596.
[21] P.D. Askouni, C. (Corina), G. Papanicolaou, Textile reinforced mortar-to-masonry bond: experimental investigation of bond-critical parameters, Constr. Build. Mater. (207 2019) 535–547, https://doi.org/10.1016/j.conbuildmat.2019.02.102.
[22] G. Ferrara, M. Pepe, E. Martinelli, R. Dias, Tensile behavior of flax textile reinforced lime-mortar : Influence of reinforcement amount and textile impregnation, 119 (2021). https://doi.org/10.1016/j.cemconcomp.2021.103984.
[23] S. Mazzuca, H.A. Hadad, L. Ombres, A. Nanni, Mechanical characterization of steel-reinforced grout for strengthening of existing masonry and concrete structures, J. Mater. Civ. Eng. 31 (2019) 04019037, https://doi.org/10.1061/(ASCE)MT.1943-5533.0002669.
[24] D. De Domenico, A. Quattrocchi, D. Alizzio, R. Montanini, S. Urso, G. Ricciardi, A. Recupero, Experimental characterization of the FRCM-concrete interface bond behavior assisted by digital image correlation, Sensors (Switzerland) 21 (2021) 1–20, https://doi.org/10.3390/s21041154.

[25] S. Pavía, R. Hanley, Flexural bond strength of natural hydraulic lime mortar and clay brick, Mater. Struct. 43 (2010) 913–922, https://doi.org/10.1617/s11527-009-9555-2.
[26] Z. Zhou, Development of bond strength in hydraulic lime mortared brickwork, University of Bath, 2012.
[27] E. Vitale, D. Deneele, M. Paris, G. Russo, Multi-scale analysis and time evolution of pozzolanic activity of lime treated clays, Appl. Clay Sci. 141 (2017) 36–45, https://doi.org/10.1016/j.clay.2017.02.013.
[28] F.A. Cardoso, H.C. Fernandes, R.G. Pileggi, M.A. Cincotto, V.M. John, Carbide lime and industrial hydrated lime characterization, Powder Technol. 195 (2009) 143–149, https://doi.org/10.1016/j.powtec.2009.05.017.
[29] K. Scrivener, R. Snellings, B. Lothenbach, A practical guide to microstructural analysis of cementitious materials, Taylor & Francis Group, 2016.
[30] ASTM C109/C109M-05, Standard test method for compressive strength of hydraulic cement mortars (Using 2-in. or [50-mm] Cube Specimens), 2005. https://doi.org/10.1520/C0109_C0109M-05.
[31] BS EN 1015-11, Methods of test for mortar for masonry. Determination of flexural and compressive strength of hardened mortar, 1999.
[32] BS EN 12390-13, Testing hardened concrete. Determination of secant modulus of elasticity in compression, 2013.
[33] ASTM C496/C496M- 04, Standard test method for splitting tensile strength of cylindrical concrete specimens, 2004. https://doi.org/10.1520/C0496_C0496M-04.
[34] ASTM C67-05, Standard test methods for smpling and testing brick and structural clay tile, 2005. https://doi.org/10.1520/C0067_C0067M-20.
[35] BS EN 1015-18, Methods of test for mortar for masonry- Determination of water absorption coefficient due to capillary action of hardened mortar, 2002.
[36] BS EN 772-11, Methods of test for masonry units. Determination of water absorption of aggregate concrete, autoclaved aerated concrete, manufactured stone and natural stone masonry units due to capillary action and the IRA of clay masonry units, 2011.
[37] BS EN 12617-4, products and systems for the protection and repair of concrete structures. Test methods, Determination of Shrinkage and Expansion, 2002.
[38] A. Dalalbashi, B. Ghiassi, D.V. Oliveira, A. Freitas, Effect of test setup on the fiber-to-mortar pull-out response in TRM composites: experimental and analytical modeling, Compos. B Eng. 143 (2018) 250–268, https://doi.org/10.1016/j.compositesb.2018.02.010.
[39] A. Dalalbashi, B. Ghiassi, D.V. Oliveira, A multi-level investigation on the mechanical response of TRM-strengthened masonry, Mater. Struct. 54 (2021), https://doi.org/10.1617/s11527-021-01817-4.
[40] G. Ye, X. Liu, G. De Schutter, A.-M. Poppe, L. Taerwe, Influence of limestone powder used as filler in SCC on hydration and microstructure of cement pastes, Cem. Concr. Compos. 29 (2007) 94–102, https://doi.org/10.1016/j.cemconcomp.2006.09.003.
[41] J.D.A.M. Filho, F.D.A. Silva, R.D. Toledo Filho, Degradation kinetics and aging mechanisms on sisal fiber cement composite systems, Cem. Concr. Compos. 40 (2013) 30–39, https://doi.org/10.1016/j.cemconcomp.2013.04.003.
[42] A. El-Turki, R.J. Ball, S. Holmes, W.J. Allen, G.C. Allen, Environmental cycling and laboratory testing to evaluate the significance of moisture control for lime mortars, Constr. Build. Mater. 24 (2010) 1392–1397, https://doi.org/10.1016/j.conbuildmat.2010.01.019.
[43] J. Lanas, J. Perez Bernal, M.A. Bello, J.I. Alvarez Galindo, Mechanical properties of natural hydraulic lime-based mortars, Cem. Concr. Res. 34 (2004) 2191–2201, https://doi.org/10.1016/j.cemconres.2004.02.005.
[44] A. Izaguirre, J. Lanas, J.I. Álvarez, Ageing of lime mortars with admixtures: Durability and strength assessment, Cem. Concr. Res. 40 (2010) 1081–1095, https://doi.org/10.1016/j.cemconres.2010.02.013.
[45] R.J. Ball, G.C. Allen, Load-dependent deformation and shrinkage in hydraulic lime mortars, Int. J. Sustain. Eng. 3 (2010) 40–46, https://doi.org/10.1080/19397030903191219.
[46] A. Duran, I. Navarro-Blasco, J.M. Fernández, J.I. Alvarez, Long-term mechanical resistance and durability of air lime mortars with large additions of nanosilica, Constr. Build. Mater. 58 (2014) 147–158.
[47] O.S. Baghabra Al-Amoudi, S. Ahmad, M. Maslehuddin, S.M.S. Khan, Lime-activation of natural pozzolan for use as supplementary cementitious material in concrete, Ain Shams Eng. J. 13 (3) (2022) 101602.
[48] A. Dalalbashi, B. Ghiassi, D.V. Oliveira, Textile-to-mortar bond behavior: An analytical study, Constr. Build. Mater. 282 (2021), 122639, https://doi.org/10.1016/j.conbuildmat.2021.122639.
[49] R.J. Ball, A. EI-Turki, W.J. Allen, J.A. Nicholson, G.C. Allen, Deformation of NHL3.5 and CL90/PC hybrid mortars, Proceedings of the Institution of Civil Engineers: Construction Materials. 162 (2009) 29–35. https://doi.org/10.1680/coma.2009.162.
[50] G. Allen, R. Ball, Mechanical Properties of Hydraulic Lime Mortars, in. 4th Portuguese Congress on Mortars and ETICS, 2012.
[51] B.V. Venkatarama Reddy, M.S. Latha, Mortar shrinkage and flexure bond strength of stabilized soil brick masonry, J. Mater. Civ. Eng. 30 (2018) 2–6, https://doi.org/10.1061/(ASCE)MT.1943-5533.0002280.
[52] K. Venu Madhava Rao, B.V. Venkatarama Reddy, K.S. Jagadish, Flexural bond strength of masonry using various blocks and mortars, Mater. Struct. 29 (2) (1996) 119–124.
[53] J.P. Forth, J.J. Brooks, S.H. Tapsir, The effect of unit water absorption on long-term movements of masonry, Cem. Concr. Compos. 22 (2000) 273–280, https://doi.org/10.1016/S0958-9465(00)00027-5.